A case study of rapid mixing across the extratropical tropopause based on Civil Aircraft for the Regular Investigation of the Atmosphere Based on an Instrumented Container (CARIBIC) observations

T. S. Rhee,[1] C. A. M. Brenninkmeijer,[1] J. Mühle,[1,2] P. F. J. van Velthoven,[3] M. Hermann,[4] A. Zahn,[5] D. E. Oram,[6] D. H. Scharffe,[1] C. Koeppel,[1] H. Fischer,[1] and J. Lelieveld[1]

Received 16 February 2005; revised 9 August 2005; accepted 7 September 2005; published 16 November 2005.

[1] Using the CARIBIC Boeing 767 aircraft, a suite of trace gases and aerosols was measured between Germany and the Maldives in June 2000 at altitudes between 9.4 and 10 km. In the extratropics, the flight track was located in the tropopause region. A large variability of trace gases and ultrafine aerosol concentrations was observed while the aircraft intercepted air masses from the upper troposphere and the lowermost stratosphere, as well as outflow of deep convection. The correlations of alkanes (C2–C5) observed in the nonconvective areas point to relatively rapid mixing across the tropopause within about a day. Unusually high mixing ratios of short-lived alkanes (C4–C6) in the convective areas indicate rapid transport of boundary layer air masses to cruising altitude. Using the ratios of the mixing ratios of alkanes (C3–C5) observed in the convective and nonconvective areas, we estimate the age of air masses in the tropopause region to be 24(±6) days for this event. This timescale is similar to that of vertical transport within the troposphere. Altogether our observations provide further evidence that the extratropical tropopause is often not a very effective mixing barrier.

Citation: Rhee, T. S., et al. (2005), A case study of rapid mixing across the extratropical tropopause based on Civil Aircraft for the Regular Investigation of the Atmosphere Based on an Instrumented Container (CARIBIC) observations, *J. Geophys. Res.*, *110*, D22301, doi:10.1029/2005JD005890.

1. Introduction

[2] The extratropical tropopause slopes downward toward the poles [*Holton et al.*, 1995] and varies in space and time [e.g., *Appenzeller et al.*, 1996]. Because of this downward slope, isentropic surfaces are intersected, in particular near the subtropical jet stream. This implies that two-way exchange between the extratropical stratosphere and the tropical upper troposphere can occur along the isentropic surfaces [e.g., *Hintsa et al.*, 1998, and references therein; *Ray et al.*, 1999]. This part of the extratropical stratosphere, which is affected by such exchange, is called the lowermost stratosphere (LMS) and is bounded by the isentropic surface of $\theta = 380$ K and the local tropopause [*Holton et al.*, 1995]. The LMS is ventilated by diabatic subsidence of stratospheric air across isentropic surfaces through "downward control" [*Haynes et al.*, 1991; *Holton et al.*, 1995] and also by adiabatic exchange with the upper troposphere (UT) [*Chen*, 1995]. Besides these two large-scale processes, tropospheric air enters the LMS by episodic upward transport driven by deep convection in the midlatitudes [*Fischer et al.*, 2003; *Lelieveld et al.*, 1997; *Poulida et al.*, 1996; *Ray et al.*, 2004].

[3] On the basis of vertical profiles of long-lived tracers, *Ray et al.* [1999] argued that the transport of tropospheric air into the LMS peaks in summer and can even reach the upper boundary of the LMS ($\theta = 380$ K), because of a weakening of the subtropical jet stream [*Chen*, 1995]. They also estimated that the transport time of tropospheric air from the Earth's surface into the LMS is less than 1.5 months. Recent observations in the UT and LMS over Europe and Canada not only confirmed the occurrence of intrusions of tropospheric air into the LMS, but also demonstrated the existence of a mixing layer in the lower part of the LMS [*Fischer et al.*, 2000; *Hoor et al.*, 2002, 2004; *Scheeren et al.*, 2003]. This mixing layer apparently wanes in winter and waxes in summer, which *Hoor et al.* [2002] attributed to the weakening of subtropical jet in summer, the same process as proposed by *Ray et al.* [1999]. *Scheeren et al.* [2003] corroborated the existence of the mixing layer up to the $\theta = 370$ K surface in summer, and estimated the age of tropospheric air inside the mixing layer to be 3–14 days. Thus observations in the LMS point to transport and mixing of air from the UT during summer. Our study aims at testing these arguments using measure-

[1]Atmospheric Chemistry Division, Max Planck Institute for Chemistry, Mainz, Germany.
[2]Now at Scripps Institution of Oceanography, University of California, San Diego, La Jolla, California, USA.
[3]Royal Netherlands Meteorological Institute (KNMI), De Bilt, Netherlands.
[4]Leibniz Institute for Tropospheric Research, Leipzig, Germany.
[5]Institute of Meteorology and Climate Research, Karlsruhe University, Karlsruhe, Germany.
[6]School of Environmental Sciences, University of East Anglia, Norwich, UK.

0148-0227/05/2005JD005890$09.00

Table 1. Photochemical Lifetimes (τ) of Selected Hydrocarbons and CO Under the Conditions of the Extratropical Section of the Flight[a]

Compound	τ, days	Reference
Ethane	154	*DeMore et al.* [1997]
Propane	23	*DeMore and Bayes* [1999]
Butane	9	*DeMore and Bayes* [1999]
Isobutane	7	*Talukdar et al.* [1994]
Pentane	5	*DeMore and Bayes* [1999]
Isopentane	5	*Atkinson* [1986]
Hexane	4	*DeMore and Bayes* [1999]
2-Methylpentane	4	*Atkinson* [1986]
3-Methylpentane	3	*Atkinson* [1986]
Cyclohexane	3	*DeMore and Bayes* [1999]
CO	67	*DeMore et al.* [1997]

[a]Photochemical lifetimes are estimated as inverse of the product of the rate constant (k) of a gas at the temperature of 225 K and the pressure of 251 mbar and the hydroxyl radical number density of 1.0×10^6 molecule cm^{-3} [*Spivakovsky et al.*, 2000].

ments of nonmethane hydrocarbons (NMHCs) in the vicinity of the extratropical tropopause obtained during a CARIBIC flight (Civil Aircraft for the Regular Investigation of the Atmosphere Based on an Instrumented Container) [*Brenninkmeijer et al.*, 1999].

[4] Because of the wide range of reactivity with OH (Table 1), the ratios of NMHCs mixing ratios have often been used to trace and to estimate the photochemical age of air masses of interest or, conversely, the OH concentration under defined conditions [e.g., *Calvert*, 1976; *Goldstein et al.*, 1995; *McKeen et al.*, 1996; *McKenna et al.*, 1995; *Parrish et al.*, 1992; *Rudolph and Johnen*, 1990]. However, these applications have been mostly limited to the planetary boundary layer or continental outflow, for which the influence of localized sources complicates the analysis [*McKeen and Liu*, 1993]. Perhaps less directly perturbed regions, such as the free troposphere and the LMS may also be interesting for the application of NMHC studies owing to the presence of relatively homogeneous background air masses [e.g., *Scheeren et al.*, 2003].

[5] To examine the physical and chemical processes occurring in the extratropical tropopause region in summer, we analyze multiple chemical tracers observed during one CARIBIC flight. Among 13 single CARIBIC flights between Germany and the Maldives or Sri Lanka for which NMHCs were analyzed [*Rhee et al.*, 2002], this flight is uniquely informative to this end, as the aircraft intersected convective and nonconvective areas along the extratropical tropopause region. In particular, the large variability of NMHCs observed in the extratropics during this flight allows us to estimate the age of air masses, and the mixing timescales in the tropopause region in summer.

2. Experiment

[6] The measurements and air sampling were carried out by the CARIBIC passenger aircraft (Boeing 767–300 ER from LTU International Airways) on 15 June 2000. Departing at 7:30 (GMT), the 9 hour (~8100 km) flight from Male, the Maldives (4.2°N, 73.7°E) to Düsseldorf, Germany (51.4°N, 6.8°E) crossed the Arabian Sea, Iran, the Black Sea, and Romania (Figure 1) at altitudes between 9.4 and 10 km (Figure 2).

[7] The automated CARIBIC instrument container has equipment for analyzing O_3, CO, and aerosol particles in situ, and for collecting 12 large-volume air samples (21 L at 17 bars) at regular intervals [*Brenninkmeijer et al.*, 1999]. The air sample collection time was 20 min (~300 km). O_3 and CO were analyzed every 17 s (~4 km) and 130 s (~32 km), respectively [*Zahn et al.*, 2002]. Three condensation particle counters measured the aerosol number concentrations in three size ranges (4 nm–1.3 μm, 12 nm–1.3 μm, and 18 nm–1.3μm) every 2 s (~0.5 km) [*Hermann and Wiedensohler*, 2001]. The number concentration of ultrafine particles is derived as the difference between the readings of the first two counters corrected to STP (N_{4-12}). On returning the container to the laboratory, the air samples were processed to analyze the isotopic composition of CO, and the mixing ratios of NMHCs, halocarbons, CO_2, CH_4, N_2O, and SF_6. To minimize the effect of sample storage, the analysis of NMHCs was done within a week of collection. Nevertheless, alkene mixing ratios were increasing in the large volume canisters, and therefore are not considered. Analytical details for NMHC measurements were described by *Mühle et al.* [2002]. Analytical uncertainties and detection limits for each compound were calculated on the basis of calibration runs at 95% confidential level [*Mitchell et al.*, 1977]. Analytical protocols for other compounds were described by *Krol et al.* [2003] for CH_3I, HCFC-22, and HCFC-141b, by *Brenninkmeijer et al.* [2001] and *Zahn et al.* [2002] for CO and O_3, by *Hermann et al.* [2001] for aerosol concentrations, by *Bergamaschi et al.* [2000] for N_2O, and by *Brenninkmeijer* [1993] for ^{14}CO analysis.

3. Meteorological Situation

[8] The description of the synoptic-scale meteorological conditions along the flight track is based on vertical cross sections of potential vorticity (PV) and potential temperature (θ) calculated from the European Centre for Medium-Range Weather Forecast (ECMWF) first guess (6 hour forecast) fields at a resolution of 1° by 1° (Figure 2). The

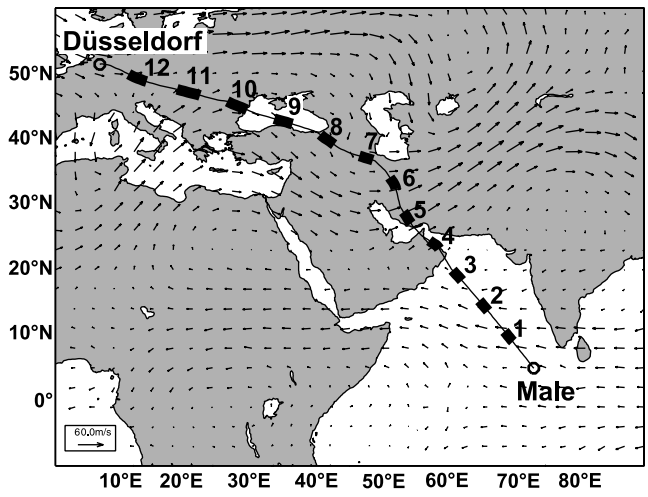

Figure 1. Flight track from Male, the Maldives, to Düsseldorf, Germany, overlying the wind vectors calculated from ECMWF data at 250 hPa at 12:00 GMT. The air sampling periods are marked as solid bars with canister numbers.

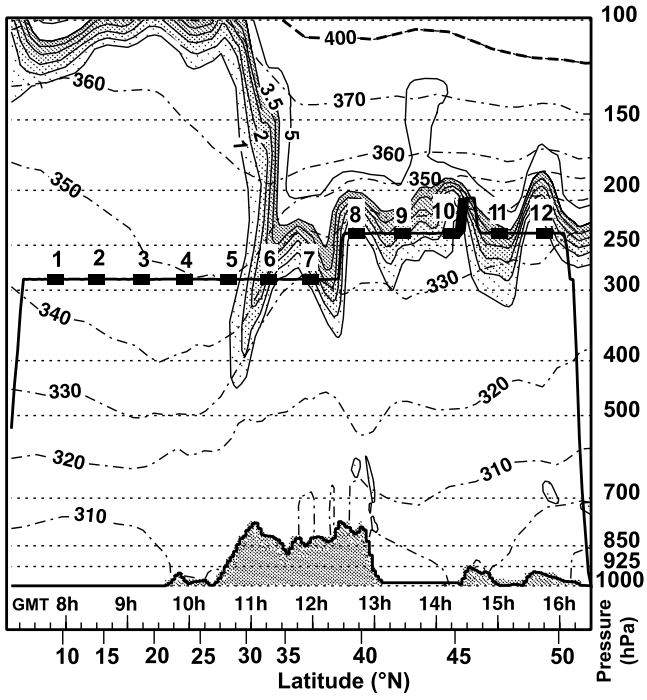

Figure 2. Vertical distribution of potential vorticity (solid line) and potential temperature (dash-dotted line) along the flight track based on an interpolation of the ECMWF data for 6:00, 12:00, and 18:00 GMT. The tropopause region between PVU = 1 and 3.5 is gradually stippled. The air sampling periods are marked as solid bars with canister numbers.

local tropopause can be diagnosed as the location of the sharp gradient in PV [e.g., *Danielsen*, 1968; *Reed*, 1955]. A number of studies have proposed different PV values to optimally represent the dynamical tropopause [*Bethan et al.*, 1996; *Hoerling et al.*, 1991; *Hoinka et al.*, 1993; *Wirth*, 2000], but consensus about this is lacking [*Danielsen et al.*, 1987; *Hoerling et al.*, 1991; *Hoinka et al.*, 1993; *Holton et al.*, 1995; *Tuck et al.*, 1985; *Zahn et al.*, 2004] and the "optimal" value may depend on season and latitude. For the present study we define the "tropopause region" by the range of 1–3.5 PVU (1 PVU = 10^{-6} $Km^2kg^{-1}s^{-1}$).

[9] As shown in Figure 2, the aircraft entered a deep tropopause fold at 30°N below the subtropical jet stream, and flew mostly in the tropopause region afterward. Hence we will use 30°N as the latitude which delimits the tropics from the extratropics. At the northwestern side of the upper level trough, the aircraft sampled another weaker fold (at ~39°N). The upper level trough was associated with a decaying upper level PV filament connecting a cutoff low centered over Sardinia, Italy, with a large trough over Kazakhstan (see http://www.knmi.nl/samenw/campaign_support/CARIBIC/150600/index.html for additional meteorological information). Between 40°N and 47°N the aircraft passed once again the upper level PV filament. At 45.5°N (14:30 GMT) the aircraft was forced to climb to avoid intense turbulence associated with a deep convective system over the Carpathian Mountains in Romania (see also satellite image in Figure 5). The irregular undulation of the tropopause therefore seems to be partly related to the deep convection that occurred before and during the flight. In particular, dense high cloud cover and a large ice water content in the clouds around this segment (ECMWF analysis) points toward recent influence by deep convection. The deep convection systems encountered during the flight will be discussed in detail below on the basis of the measurements of chemical compounds, aerosols, and satellite observations.

4. Results

4.1. Deep Convection in the Extratropics

[10] A striking feature observed in the extratropical section of the flight is the strong enhancement of short-lived alkanes, C4 to C6, between 42°N and 47°N (samples 9, 10, and 11), but not at 34°N (sample 6) and 40°N (sample 8) where high mixing ratios of relatively long lived alkanes (C1 to C3) were encountered (Figure 3). Even cyclohexane, which is usually below the detection limit, was detected at 45°N (sample 10). Since these short-lived alkanes are emitted in the boundary layer, the observation of relatively high mixing ratios points to rapid transport of boundary layer air to cruising altitude. Accounting for the "natural" dilution by entrainment of environmental air from the free troposphere during the convection event [e.g., *Fischer et al.*, 2003; *Fridlind et al.*, 2004] and by the "artificial" dilution due to the long sampling distance (~300 km), these high mixing ratios of short-lived alkanes suggest the transport of substantial amounts of polluted air from the boundary layer ("vacuum cleaner" process) [*Chatfield and Crutzen*, 1984; *Mullendore et al.*, 2005].

[11] The segment of the flight track between 42°N and 47°N also exhibits episodic increases of N_{4-12} and CO, and simultaneous decreases in O_3 (Figure 4). In particular, the two large peaks in N_{4-12} during the air sampling periods of 9 and 10 coincide with sharp decreases in O_3 and concomitant increases in CO, witnessing the recent injection of boundary layer air masses, which can trigger new particle formation in the outflow [*de Reus et al.*, 2001; *Krejci et al.*, 2003; *Ström et al.*, 1999; *Twohy et al.*, 2002]. The increase of N_{4-12} during the collection of sample 11 is not so pronounced as that observed during the sampling periods of 9 and 10, however. The corresponding mean fraction of N_{4-12} to all submicrometer particles (~10%) is lower than that for samples 9 (~20%) and 10 (~40%), suggesting that the low N_{4-12} in sample 11 may result from the rapid growing of particles in the outflow of deep convection due to a large supply of precursors (see section 4.2.3). The in situ observations of CO, O_3, and aerosol are therefore consistent with the occurrence of high mixing ratios of short-lived NMHCs between 42°N and 47°N, both of which have been driven by deep convection.

[12] There is further evidence that indicates events of deep convection. First, the variability of PV does not follow the sharp change in O_3 during the deep convection events. This is attributable to problems in properly simulating changes in mesoscale meteorology during deep convection in the ECMWF model likely due to its coarse resolution (1° by 1°). Second, the satellite visible (Figure 5) and infrared (not shown) images clearly show the presence of deep convective clouds (cumulonimbus) along the Dinaric Alps in the Balkans and over central Italy and Corsica, which

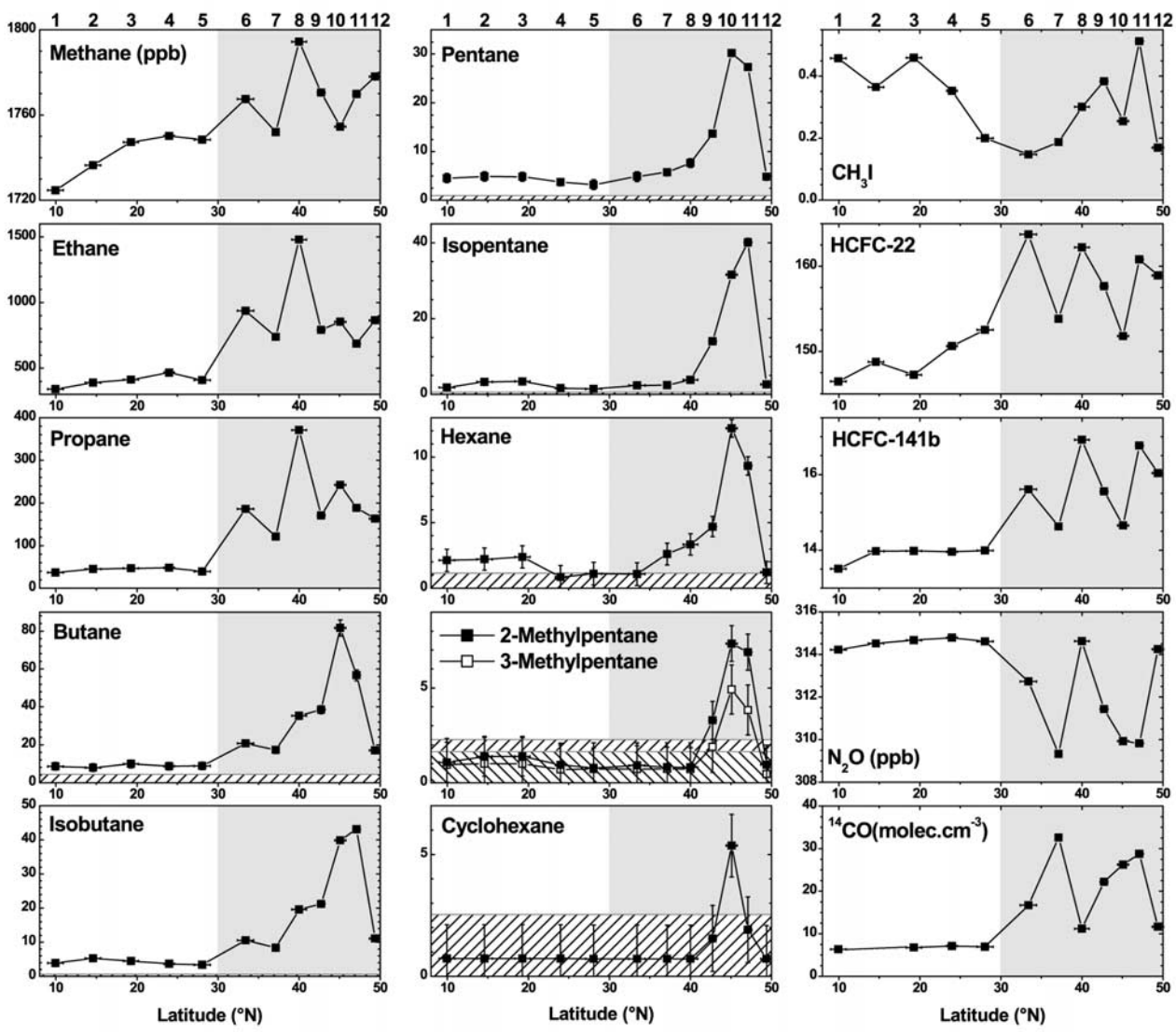

Figure 3. Spatial distribution of selected hydrocarbons and halocarbons, N_2O, and ^{14}CO. Units are ppt except for CH_4 (ppb), N_2O (ppb), and ^{14}CO (molecule cm^{-3}). Shading indicates the extratropics and hatching represents the detection limit. The canister numbers are denoted at the top. Note that the detection limit of 3-methylpentane is higher than that for 2-methylpentane. Horizontal and vertical error bars designate the sample collection period and the uncertainty of measurement at 95% confidence level, respectively.

clearly demonstrates the convective meteorological conditions along and near the flight track.

4.2. Rapid Mixing Across the Extratropical Tropopause

4.2.1. Identification of Continuous Mixing

[13] CO and O_3 together have been used as tracers for tropospheric and stratospheric air masses. In this way the transport of stratospheric air into the UT [e.g., *Hipskind et al.*, 1987] and the mixing of tropospheric air inside the LMS [e.g., *Hoor et al.*, 2002, 2004] has been diagnosed. Furthermore, a new concept of the chemical tropopause was suggested on the basis of the CO-O_3 relation [*Pan et al.*, 2004; *Zahn et al.*, 2004]. As shown by observations near the tropopause, mixing between the UT and LMS leads to linear mixing lines with negative slopes of the CO-O_3 relation, because of their different sources and sinks in the two reservoirs [*Hoor et al.*, 2002].

[14] As shown in Figure 6a, the CO-O_3 relationship for the extratropics does have a negative slope, be it with rather large scatter. This scatter can be attributed to a large variability of CO resulting from local surface emissions and to a lesser extent from its oxidation during transport. Nonetheless, the negative slope of the CO-O_3 relation suggests mixing across the tropopause to be dominant. In contrast to the large scatter in the CO-O_3 correlation, the compact curves of O_3 and ^{14}CO versus N_2O unambiguously indicate a continuous mixing between the UT and LMS in the extratropical tropopause region (Figures 6b and 6c). N_2O is emitted at the surface and is destroyed in the stratosphere by photolysis and reaction with $O(^1D)$, while O_3 and ^{14}CO are predominantly produced in the strato-

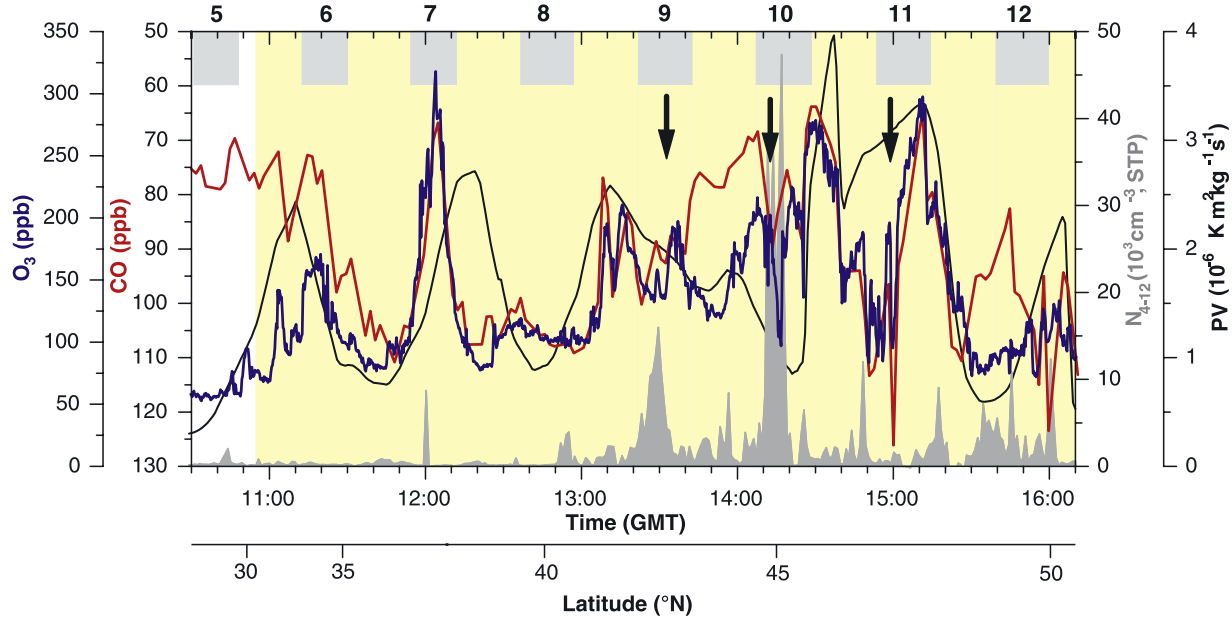

Figure 4. Time series of O_3 (blue line), CO (inverse scale, red line), ultrafine aerosol (N_{4-12}) (gray filled), and potential vorticity calculated from ECMWF data (black line) along the flight track. Arrows indicate pronounced deep convection events. Yellow shading indicates the extratropics, and gray bars at the top indicate the air sampling periods.

sphere and destroyed in the troposphere. These three tracers are distributed relatively homogeneously in the UT and LMS, and therefore are well suited for mixing diagnosis. Even the data points obtained in the convective areas (samples 9, 10, and 11) lie on the linear mixing line of data observed in the nonconvective areas.

4.2.2. Correlation Between Alkanes Observed in Nonconvective Areas

[15] Analyzing the spatial or temporal distribution of trace gases with a similar life cycle but different lifetimes provides insight into the roles of chemistry and mixing. Alkanes are the best known example, being generally emitted from common sources and removed by reaction with OH at different rates. This property has been used to estimate the concentration of OH or the photochemical age of an air mass. In a Lagrangian framework the rate of change in mixing ratio of a tracer is given by [*McKeen and Liu*, 1993, and references therein; *McKeen et al.*, 1990]:

$$\frac{dX}{dt} = -\Lambda_x X - \Psi(X - X_B) \tag{1}$$

where X and X_B are actual and background mixing ratios respectively, while Λ_x and Ψ denote the chemical loss and mixing rates. The chemical loss rate is the product of the rate constant of a compound and the OH concentration (its inverse equals the lifetime of a chemical species). Assuming that Λ_x and Ψ are constant, one can derive the analytical solution [see also *McKeen and Liu*, 1993]:

$$X = \frac{\Psi X_B}{\Psi + \Lambda_x} + \left(X_0 - \frac{\Psi X_B}{\Psi + \Lambda_x}\right) e^{-(\Lambda_x + \Psi)t} \tag{2a}$$

or:

$$X' = X'_0 e^{-K_x t} \tag{2b}$$

where

$$X' = X - \frac{\Psi X_B}{\Psi + \Lambda_x} \tag{3}$$

$$K_x = \Lambda_x + \Psi \tag{4}$$

Equation (2) can also be used for another compound, Y with a different chemical loss rate and background mixing ratios. Combining the equations for X and Y results in:

$$\ln Y' = \left(\ln Y'_0 - \frac{K_y}{K_x} \ln X'_0\right) + \frac{K_y}{K_x} \ln X' \tag{5}$$

Note that *McKeen et al.* [1996] have derived an equation similar to (5) while assuming the background mixing ratios to be zero, unlike the present expression. In the absence of mixing, equation (5) yields the slope K_y/K_x as the ratio of the rate constants. When mixing dominates, however, the logarithm of the mixing ratios of the two compounds obeys a one-to-one relation, independent of their chemical lifetimes. Thus, by exploring this relationship one can infer the extent to which each of these two processes controls the atmospheric variability of the trace gases considered.

[16] As shown in Figure 7, the least squares fits (black dotted lines) for the alkanes observed in the nonconvective areas (samples 6, 7, 8, and 12) result in a slope of ~0.6 to ~1.6. The large difference from the photochemical oxidation line (black solid lines) points to the dominance of mixing. The scenarios with different background mixing ratios show clearly that photochemistry is of little importance (see several scenarios shown in Figure 7). Thus it can be concluded that mixing is a major process controlling the

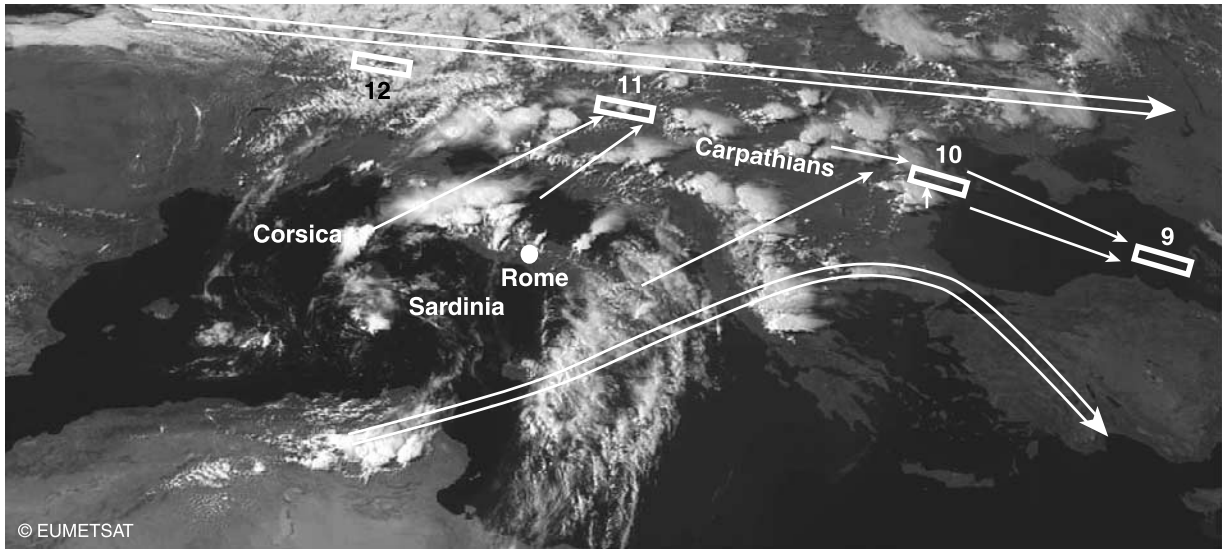

Figure 5. Meteosat-5 visible image obtained at 15:00 (GMT) (EUMETSAT, Darmstadt, Germany). Double line arrows indicate the midlatitude jet (north) and the subtropical jet (south) streams. Single line arrows indicate deep convection outflow on the basis of the ECMWF wind map (Figure 1) and the image shown. Rectangular boxes indicate the air sampling locations of 9, 10, 11, and 12.

distribution of the NMHCs observed in the nonconvective extratropical tropopause region.

[17] To approximate the rate of mixing, we applied 3-day (blue dashed lines) and 15-day (red dashed lines) mixing timescales to the model, implying that the slope (K_y/K_x) in equation (5) is not necessarily one. These two timescales bracket the range of transport times from the troposphere to the mixing layer of the LMS as estimated by *Scheeren et al.* [2003] (see Figure 10). As shown by the correlation of propane and ethane in Figure 7, the data points obtained in the mixing layer of the LMS by *Scheeren et al.* [2003] ("TSE events") indeed follow the model scenarios with these mixing timescales, indicating consistency between the two calculations. All correlations of the alkanes, except that for propane, clearly show that the mixing time in the tropopause region was less than 3 days for this flight.

[18] *Scheeren et al.* [2003] measured NMHCs of air samples collected at the altitudes of 7.5 to ~13 km spanning from the UT to the LMS. Defining the tropopause at an O_3 mixing ratio of 120 ppbv in conjunction with a potential vorticity of 3.5 PVU, they grouped their measurements into the UT, the mixing layer of the LMS, and the LMS. The upper boundary of the mixing layer was defined at 30 K higher than the potential temperature at the tropopause, in accord with *Hoor et al.* [2002]. The results of the summer campaign in July 1998 are shown in Figure 7. Note that, in terms of potential vorticity, their choice of tropopause forms an upper boundary to the tropopause region we defined (1–3.5 PVU) and lies within the tropopause region on the basis of the O_3 mixing ratio (Figure 6a). This is quite consistent because the range of NMHCs for the UT overlaps with our measurements in the tropopause region. The interesting point is that in Figure 7, *Scheeren et al.*'s [2003] mean values of NMHCs observed in the mixing layer of the LMS indicate mixing dominance comparing with the values of the UT. Although the large variability of measurements and

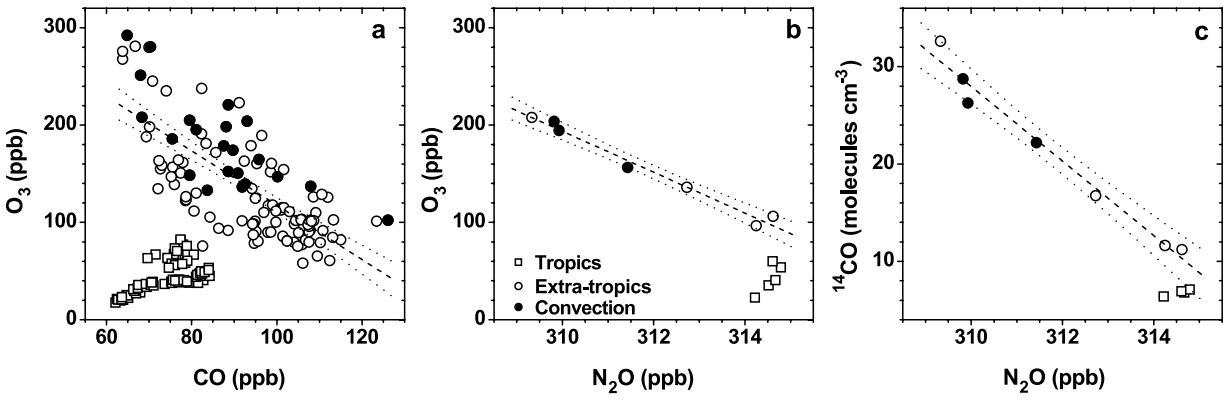

Figure 6. Correlations of (a) O_3 versus CO, (b) O_3 versus N_2O, and (c) ^{14}CO versus N_2O. Symbol keys are shown in Figure 6b. Mean O_3 mixing ratios for the air sampling segments are used in Figure 6b. Dashed lines are the least squares fits for all data obtained in the extratropics and dotted lines indicate the confidence bands at 95% probability.

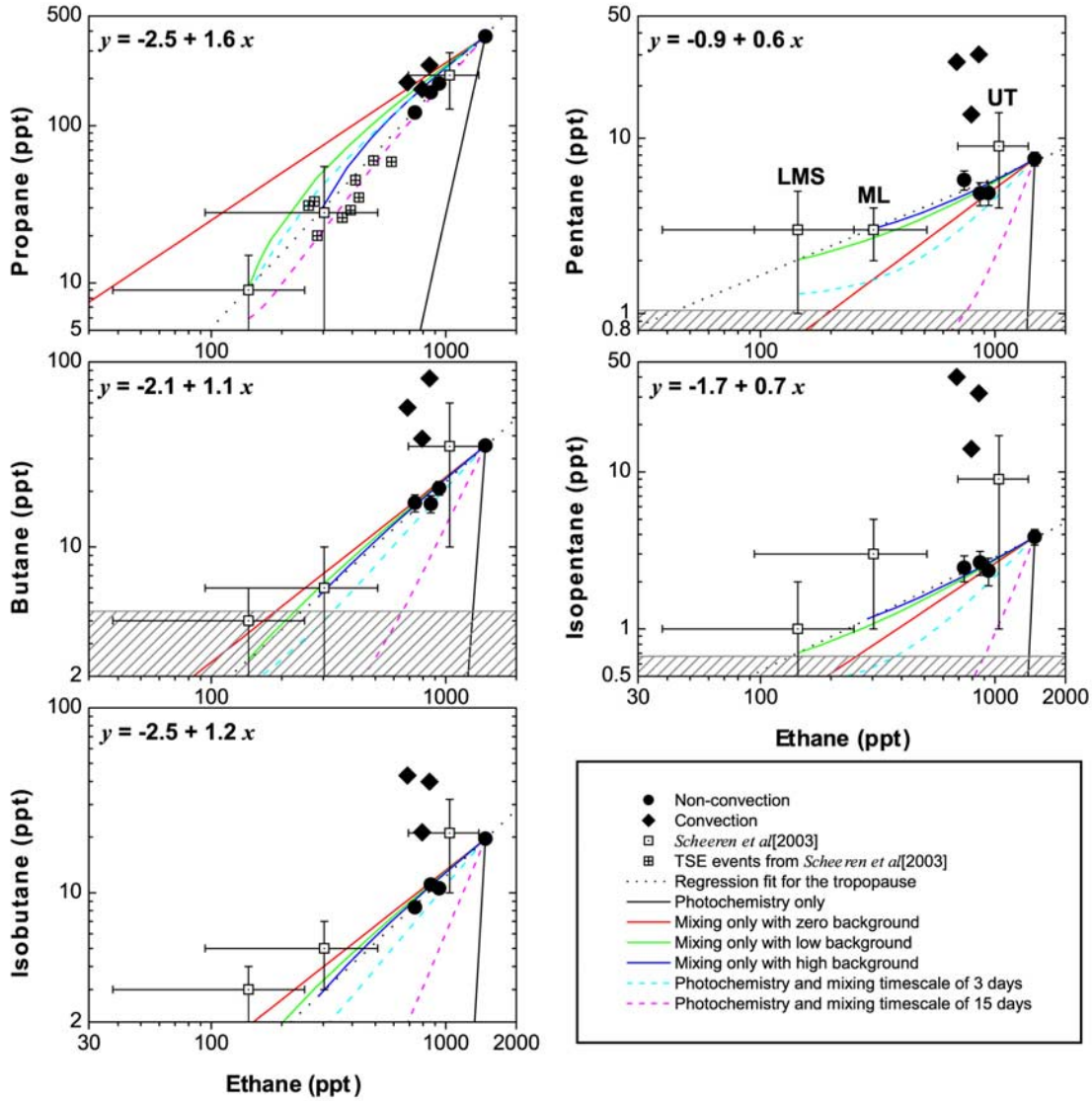

Figure 7. Correlations between selected alkanes and ethane from observations and model simulations. The regression equations are shown in the corner. Linear regressions are calculated with weighting uncertainties for the baseline data. As indicated in the index box, six scenarios of model simulations are plotted. Three background mixing ratios of ethane were prescribed: zero, low background matching the value observed in the LMS by *Scheeren et al.* [2003] (144 ppt), and high background being twice that (288 ppt). Those of the other alkanes were calculated by inserting the ethane background values to the least squares fits. The data points of *Scheeren et al.* [2003] are taken from their Table 2 for the upper troposphere (UT), the mixing layer (ML: $\Delta\theta = 0 - 30$ K), and the LMS ($\Delta\theta > 30$ K) in July 1998, and TSE (troposphere-to-stratosphere exchange) events are taken from their Table 5. Gray hatching represents the detection limits of our instrument for the compounds.

the low mixing ratios of short-lived NMHCs (near the detection limit) in the mixing layer reduce the significance of the mean values, it suggests considerable influence of mixing on the distribution of NMHCs in the mixing layer of the LMS in summer, which *Scheeren et al.* [2003] also argued on the basis of the transport timescales of the tropospheric air masses. Therefore application of (5) appears to be useful to discriminate physical and chemical processes occurring in the region of the tropopause and the LMS.

[19] We further confine the mixing timescale based on the slope in equation (5). Since the mixing line extends to the short-lived isopentane, the mixing timescale must be smaller than that for the photochemical oxidation of isopentane. Since the photochemical lifetime of ethane is ~30 times that of isopentane (Table 1), the slope becomes:

$$\frac{K_{iC5H12}}{K_{C2H6}} = \frac{\Lambda_{iC5H12} + \Psi}{\Lambda_{C2H6} + \Psi} \approx 1 + \frac{\Lambda_{iC5H12}}{\Psi} \quad (6)$$

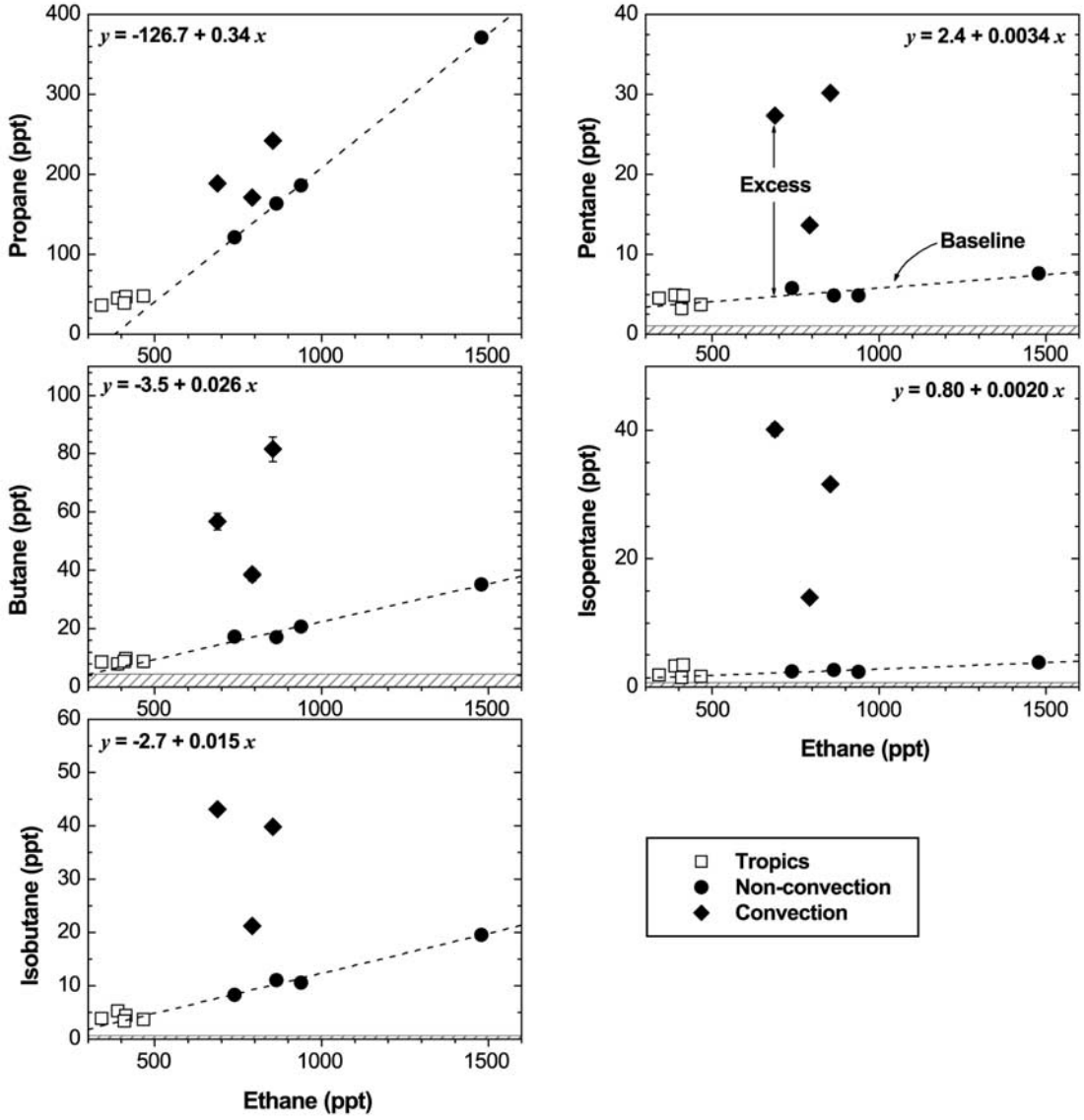

Figure 8. Scatterplots of the selected alkanes and ethane. Shown are the baseline relations and the graphical definition of "excess" mixing ratios. The regression equations for the baseline are presented in each panel. Shaded hatching represents the detection limits.

When defining the upper limit of the mixing timescale at $1/e^2$ of photochemical lifetime of isopentane, we obtain:

$$\frac{K_{iC5H12}}{K_{C2H6}} \leq 1 + e^{-2} \tag{7}$$

Accordingly, we expect mixing timescales of less than 0.7 days in the extratropical tropopause region in summer. A sensitivity test to the OH concentration shows that the upper limit of the mixing timescale varies by one day for assumed OH concentrations of 0.5 to 1.5 $\times$ 10^6 molecule cm^{-3}.

4.2.3. Chemical Clock

[20] The occurrence of unusually high mixing ratios of short-lived alkanes over the convective areas (samples 9, 10, and 11) provides additional evidence of rapid mixing across the tropopause between the UT and the LMS. To this end, we first constrain the alkane sources feeding into the air parcels in the convective areas, and next estimate the age of air masses at the extratropical tropopause.

[21] As mentioned earlier, the chemical compositions of the air samples collected in the convective areas represent a combination of the air masses lifted from the boundary layer, those entrained in the free troposphere, and those stayed in the tropopause region. When the volume fraction of the boundary layer air mass in the air sample is f, the observed mixing ratio of a compound (X) can be described as:

$$X = f X_{BL} + (1 - f) X_T \tag{8}$$

The subscript BL designates the boundary layer, and T the free troposphere plus the tropopause region. Since the fraction of the boundary air mass for other compounds (Y) should be the same, we derive the following relationship

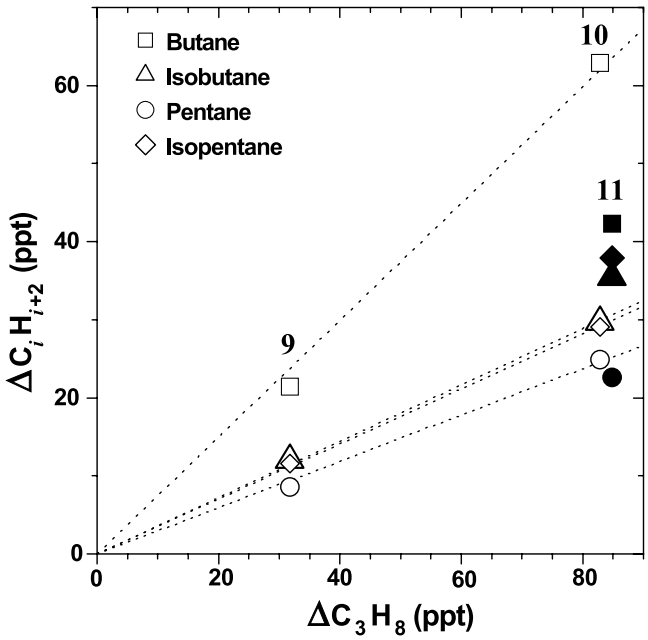

Figure 9. Correlations of the excess alkanes observed in the convective areas. Open symbols are for sample 9 and 10, and solid symbols are for sample 11.

between the observed mixing ratios and that in the boundary layer:

$$\frac{X - X_T}{Y - Y_T} = \frac{X_{BL} - X_T}{Y_{BL} - Y_T} \tag{9}$$

If the mixing ratio of a compound in the boundary layer is much larger than that in the free troposphere and the tropopause region, the right-hand side of (9) becomes the ratio of the mixing ratios of compounds in the boundary layer. Thus, provided that the NMHCs in the nonconvective areas represent that in the tropopause region and the free troposphere, the ratios of the NMHCs in the boundary layer can be derived. As illustrated in Figure 8, we define the "excess" mixing ratio as the difference in alkane mixing ratios between the observed and the "baseline" mixing ratio in the tropopause region. The latter is determined by the least squares fits between the alkanes and ethane observed in the nonconvective areas.

[22] As shown in Figure 9, the excess alkanes in samples 9 and 10 are highly correlated, although we forced the regression fits to the origin by the definition of the excess mixing ratio. However, the excess alkanes for sample 11 do not fall on these lines, suggesting that the air masses encountered during the collection of sample 9 and 10 are similar, but different from that of sample 11. Accounting for the high mixing ratios of HCFC-22 and HCFC-141b (new refrigerants replacing CFC compounds), and CH_3I (a marker for oceanic emissions [*Bell et al.*, 2002]) in sample 11 (see Figure 3), we expect that the air masses for sample 11 had originated in industrial and/or urban areas near the Mediterranean Sea. This also complies with the scenario that abundant amounts of anthropogenic SO_2 might accelerate the growth of new particles, leading to the reduced fraction of N_{4-12} in submicron aerosol concentration as observed during the sampling of 11. Indeed, the satellite visible image (Figure 5) shows large cumulonimbus clouds over Corsica and central Italy, of which the outflows are directed toward the flight track near the segment of sample 11. In contrast, the air sampling segment 10 is located at deep convective outflows over the Carpathian Mountains, and these outflows reach toward segment 9 (see wind vectors in Figure 1). The ratios of the excess alkanes are compared with those from two characteristic source categories, namely rural and urban environments [*Goldstein et al.*, 1995; *Warneck*, 1999] (Table 2). This direct comparison indicates that the ratios of the excess NMHCs straddle between the values observed in those two environments. This supports strongly that the ratios of excess NMHCs represent the source signatures of NMHCs as expressed in (9).

[23] By the definition of the "excess" and "baseline" alkane, we may assume the background mixing ratios to be zero in (2), which leads to a simple form of the exponential decay of the excess alkane to the baseline alkane due to mixing and chemical reaction. Taking the ratio of the "excess" alkanes, the age of air in the tropopause region (τ_{TP}) corresponds simply to the chemical relaxation time for which the ratio of the excess alkanes collapses to that of the baseline mixing ratios:

$$\left(\frac{X}{Y}\right)_{\text{Baseline}} = \left(\frac{X}{Y}\right)_{\text{Excess}} e^{-(\Lambda_x - \Lambda_y)\tau_{TP}} \tag{10}$$

Table 3 lists the values of τ_{TP} that are calculated by applying two sources from the Carpathian Mountains

Table 2. Comparison of the Ratios of Alkane to Propane ($\Delta Ci/\Delta C_3H_8$) for Emissions in Rural and Urban Environments and for the Excess Alkanes in Samples 9 and 10, and 11[a]

	Rural Areas		Urban Areas		CARIBIC	
Ci	*Warneck* [1999]	*Goldstein et al.* [1995]	*Warneck* [1999]	*Goldstein et al.* [1995]	9, 10	11
Butane	0.26 ± 0.07	0.44 ± 0.01	0.77 ± 0.23	0.63 ± 0.07	0.75 ± 0.03	0.50
Isobutane	0.16 ± 0.03	0.22 ± 0.01	0.46 ± 0.06	0.30 ± 0.04	0.36 ± 0.01	0.42
Pentane	0.21 ± 0.01	0.12 ± 0.01	0.35 ± 0.16	0.29 ± 0.03	0.30 ± 0.01	0.27
Isopentane	0.30 ± 0.04		0.60 ± 0.27		0.35 ± 0.01	0.45

[a]*Warneck* [1999, Table 6.8] compiled remote, rural environmental measurements from nine references, and here we left out the results from the measurement in citrus groves by *Lonneman et al.* [1978], the observation during high O_3 by *Colbeck and Harrison* [1985], and winter observations. The annual background observations at Harvard forest by *Goldstein et al.* [1995, Table 1b] were used for another set of rural emissions. The alkane ratios of urban areas were estimated from the compilation given by *Warneck* [1999, Table 6.2] and from *Goldstein et al.* [1995, Table 1a].

Table 3. Ages of Air (τ_{TP}) at the Tropopause Determined by Using the Ratios of Selected Alkanes (C_i) to Propane[a]

	$\Delta C_i/\Delta C_3H_8$, ppt ppt^{-1}			τ_{TP}, days	
C_i	Baseline	9, 10	11	9, 10	11
Butane	0.078 ± 0.010	0.75 ± 0.03	0.50	31 ± 4	25 ± 3
Isobutane	0.045 ± 0.004	0.361 ± 0.006	0.42	22 ± 2	24 ± 2
Pentane	0.010 ± 0.004	0.30 ± 0.01	0.27	21 ± 10	20 ± 9
Isopentane	0.006 ± 0.001	0.353 ± 0.005	0.45	24 ± 6	25 ± 7
Mean				24 ± 6	24 ± 5

[a]For the calculation, an atmospheric mean temperature of 240 K and an OH concentration of 1×10^6 molecule cm^{-3} were assumed.

(samples 9 and 10) and the Mediterranean coast (sample 11), and different sets of alkanes. Whichever source at a given pair of alkanes is used, the calculated values are the same within their uncertainty. Averaging the values in Table 3 provides a mean age of air in the tropopause region of 24(±6) days during this flight. When applying the ratios of NMHCs at the boundary layer compiled in Table 2, the mean ages of air in the tropopause region result in 18(±6) and 25(±9) days on the basis of the rural and urban emissions, respectively. While the direct comparison of the mean ages alludes to the occurrence of deep convection over urban areas, large uncertainty of the estimated mean ages does not allow us to clearly indicate the source.

5. Discussion and Conclusions

[24] It has been shown that deep convection can be an effective pathway to transport polluted air from the boundary layer to the UT and even into the LMS, with consequences for atmospheric chemistry [*Dickerson et al.*, 1987; *Ferek et al.*, 1986; *Lawrence et al.*, 2003; *Lelieveld and Crutzen*, 1994; *Prather and Jacob*, 1997; *Wang and Prinn*, 2000]. The present study confirms these observations and model simulations to the extent that remarkably high mixing ratios of the short-lived compounds (C4–C6) were observed in the extratropical tropopause region.

[25] Seasonal observations in the LMS have suggested the enhancement of troposphere to stratosphere exchange in summer and the increase of its intensity close to the extratropical tropopause. For instance, by investigating the SAGE II data, *Pan et al.* [1997] found a maximum of 50 ppm water vapor in summer in the lower part of the LMS (θ = 320 K) being 4–5 times higher than the mixing ratios in other seasons at the same isentropic surface, and also higher than at higher isentropic surfaces. *Hoor et al.* [2002] obtained similar results using CO-O_3 correlations of data from the UT/LMS region, showing that their linear mixing line reached up to higher isentropic surfaces in summer than in winter. These findings were attributed to the weaker subtropical jet in summer and the influence of the northern hemisphere summer monsoon, as predicted by model studies [*Chen*, 1995; *Dethof et al.*, 2000]. The same model studies also showed that stratosphere-troposphere exchange occurs vigorously on and below the isentropic surfaces of 330–340 K throughout all seasons, and that the exchange decreases with isentropic depth from the extratropical tropopause. Our observations in the tropopause region, i.e., at the isentropic surfaces of 330–350 K (Figure 2), provide an example of such strong mixing, as based on a single though detailed measurement flight in summer. It will be useful to extend such analyses to other seasons.

[26] Several transport timescales reported in the literature and estimated in this study are illustrated in Figure 10. The estimates of mixing timescales and the age of air in the tropopause region form a consistent picture with the other transport timescales. We calculated the age of air in the extratropical tropopause region to be 24(±6) days. This timescale is similar to, or less than that of vertical transport in the troposphere, 1–1.2 month [*Warneck*, 1999]. Actually this value is based on the mean vertical profiles of ^{222}Rn observed in 1960s and 1970s in all seasons. *Liu et al.* [1984], who compiled these data, separated them seasonally and found the vertical eddy diffusion coefficient to be larger in summer than in other seasons, likely because of the increasing frequency of convective activity. Therefore the lower limit of the vertical transport timescale, ~1 month, may be representative of summer conditions. Providing that a rapid mixing across the tropical tropopause occurs within about a day, our estimate of the age of air in the extratropical tropopause region agrees with the vertical transport time in the troposphere in summer.

[27] *Scheeren et al.* [2003] estimated the age of individual air parcels at 3–14 days in the mixing layer after crossing the tropopause, which is longer than the mixing time across the tropopause. Since the mixing layer was located above

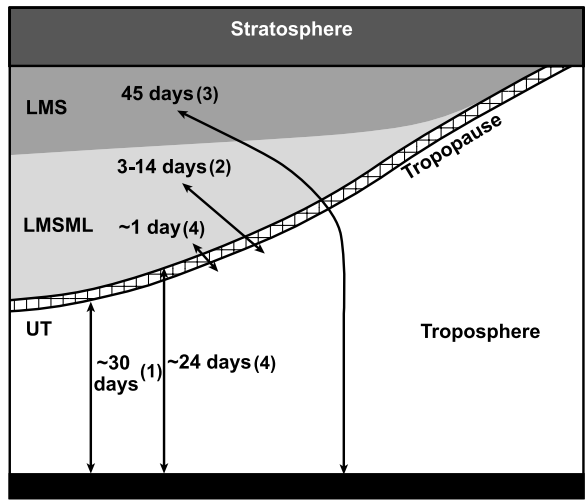

Figure 10. Schematic representation of transport timescales in the troposphere and the lowermost stratosphere. The values are from (1) *Warneck* [1999], (2) *Scheeren et al.* [2003], (3) *Ray et al.* [1999], and (4) this study. LMS, LMSML, and UT denote the lowermost stratosphere, the mixing layer in the lowermost stratosphere, and the upper troposphere, respectively.

the 330 K isentropic surface near the core of the subtropical jet stream, it is expected that troposphere to stratosphere exchange is hindered by a strong gradient of potential vorticity [*Chen*, 1995]. This probably leads to longer transport times, although this barrier effect is the least in summer. This transport time is capped by the upper limit of *Ray et al.* [1999], who estimated it to be ~1.5 month from the boundary layer to the LMS using the seasonality of CO_2 and SF_6 (thus ~15 days from the local tropopause to the LMS accounting for ~1 month vertical transport in the troposphere). Note that the estimated transport timescales by *Ray et al.* [1999] and *Scheeren et al.* [2003] are based on summer campaigns, like this study. The intensity of troposphere to stratosphere exchange therefore seems to decline with the increase of potential temperature, as predicted by *Chen* [1995] and *Dethof et al.* [2000].

[28] In conclusion, the dynamical tropopause in the extratropics in summer does not appear to be a transport barrier, but rather to be part of a transient mixing layer between the UT and the LMS. Although this conclusion is based on the observations from one CARIBIC flight, it seems to corroborate other observations in the UT/LMS region in summer and model studies as discussed above. Since the CARIBIC flights not only covered from the central Europe to the Indian Ocean, but also to the Caribbean Sea and to South Africa [*Zahn et al.*, 2002], it will be worthwhile to apply our analysis to other flight regions.

[29] **Acknowledgments.** We thank F. Slemr for comments on the manuscript and EUMETSAT (Darmstadt, Germany) for providing the Meteosat-5 satellite images. We gratefully acknowledge support through grants from the Environmental Technologies RTD program of the Commission of the European Communities DG XII (ENV4-CT95-0006 and EVK2-2001-00007) and the German Ministry for Education and Research (BMBF contract 07ATF17, AFO2000). We thank LTU International Airway for supporting the first phase of CARIBIC.

References

Appenzeller, C., J. R. Holton, and K. H. Rosenlof (1996), Seasonal variation of mass transport across the tropopause, *J. Geophys. Res.*, *101*(D10), 15,071–15,078.

Atkinson, R. (1986), Kinetics and mechanisms of the gas-phase reactions of the hydroxyl radical with organic compounds under atmospheric conditions, *Chem. Rev.*, *86*(1), 69–201.

Bell, N., L. Hsu, D. J. Jacob, M. G. Schultz, D. R. Blake, J. H. Butler, D. B. King, J. M. Lobert, and E. Maier-Reimer (2002), Methyl iodide: Atmospheric budget and use as a tracer of marine convection in global models, *J. Geophys. Res.*, *107*(D17), 4340, doi:10.1029/2001JD001151.

Bergamaschi, P., M. Bräunlich, T. Marik, and C. A. M. Brenninkmeijer (2000), Measurements of carbon and hydrogen isotopes of atmospheric methane at Izãna, Tenerife: Seasonal cycles and synoptic-scale variations, *J. Geophys. Res.*, *105*(D11), 14,531–14,546.

Bethan, S., G. Vaughan, and S. J. Reid (1996), A comparison of ozone and thermal tropopause heights and the impact of tropopause definition on quantifying the ozone content of the troposphere, *Q. J. R. Meteorol. Soc.*, *122*(532), 929–944.

Brenninkmeijer, C. A. M. (1993), Measurement of the abundance of ^{14}CO in the atmosphere and the $^{13}C/^{12}C$ and $^{18}O/^{16}O$ ratio of atmospheric CO with applications in New Zealand and Antarctica, *J. Geophys. Res.*, *98*(D6), 10,595–10,614.

Brenninkmeijer, C. A. M., et al. (1999), CARIBIC—Civil aircraft for global measurement of trace gases and aerosols in the tropopause region, *J. Atmos. Oceanic Technol.*, *16*(10), 1373–1383.

Brenninkmeijer, C. A. M., C. Koeppel, T. Röckmann, D. S. Scharffe, M. Bräunlich, and V. Gros (2001), Absolute measurement of the abundance of atmospheric carbon monoxide, *J. Geophys. Res.*, *106*(D9), 10,003–10,010.

Calvert, J. G. (1976), Hydrocarbon involvement in photochemical smog formation in Los Angeles atmosphere, *Environ. Sci. Technol.*, *10*(3), 256–262.

Chatfield, R. B., and P. J. Crutzen (1984), Sulfur dioxide in remote oceanic air: Cloud transport of reactive precursors, *J. Geophys. Res.*, *89*(D5), 7111–7132.

Chen, P. (1995), Isentropic cross-tropopause mass exchange in the extratropics, *J. Geophys. Res.*, *100*(D8), 16,661–16,673.

Colbeck, I., and R. M. Harrison (1985), The concentrations of specific C_2-C_6 hydrocarbons in the air of northwest England, *Atmos. Environ.*, *19*(11), 1899–1904.

Danielsen, E. F. (1968), Stratospheric-tropospheric exchange based on radioactivity, ozone, and potential vorticity, *J. Atmos. Sci.*, *25*(3), 502–518.

Danielsen, E. F., R. S. Hipskind, S. E. Gaines, G. W. Sachse, G. L. Gregory, and G. F. Hill (1987), Three-dimensional analysis of potential vorticity associated with tropopause folds and observed variations of ozone and carbon monoxide, *J. Geophys. Res.*, *92*(D2), 2103–2111.

DeMore, W. B., and K. D. Bayes (1999), Rate constants for the reactions of hydroxyl radical with several alkanes, cycloalkanes, and dimethyl ether, *J. Phys. Chem.*, *103*(15), 2649–2654.

DeMore, W. B., S. P. Sander, D. M. Golden, R. F. Hampson, M. J. Kurylo, C. J. Howard, A. R. Ravishankara, C. E. Kolb, and M. J. Molina (1997), Chemical kinetics and photochemical data for use in stratospheric modeling, *JPL Publ. 97-4*, 269 pp., NASA Jet Propul. Lab., Pasadena, Calif.

de Reus, M., R. Krejci, J. Williams, H. Fischer, R. Scheele, and J. Strom (2001), Vertical and horizontal distributions of the aerosol number concentration and size distribution over the northern Indian Ocean, *J. Geophys. Res.*, *106*(D22), 28,629–28,641.

Dethof, A., A. O'Neill, and J. Slingo (2000), Quantification of the isentropic mass transport across the dynamical tropopause, *J. Geophys. Res.*, *105*(D10), 12,279–12,293.

Dickerson, R. R., et al. (1987), Thunderstorms: An important mechanism in the transport of air pollutants, *Science*, *235*(4787), 460–464.

Ferek, R. J., R. B. Chatfield, and M. O. Andreae (1986), Vertical distribution of dimethylsulphide in the marine atmosphere, *Nature*, *320*, 514–516.

Fischer, H., F. G. Wienhold, P. Hoor, O. Bujok, C. Schiller, P. Siegmund, M. Ambaum, H. A. Scheeren, and J. Lelieveld (2000), Tracer correlations in the northern high latitude lowermost stratosphere: Influence of cross-tropopause mass exchange, *Geophys. Res. Lett.*, *27*(1), 97–100.

Fischer, H., et al. (2003), Deep convective injection of boundary layer air into the lowermost stratosphere at midlatitudes, *Atmos. Chem. Phys.*, *3*, 739–745.

Fridlind, A. M., et al. (2004), Evidence for the predominance of mid-tropospheric aerosols as subtropical anvil cloud nuclei, *Science*, *304*(5671), 718–722.

Goldstein, A. H., S. C. Wofsy, and C. M. Spivakovsky (1995), Seasonal variations of nonmethane hydrocarbons in rural New England: Constraints on OH concentrations in northern midlatitudes, *J. Geophys. Res.*, *100*(D10), 21,023–21,033.

Haynes, P. H., C. J. Marks, M. E. McIntyre, T. G. Shepherd, and K. P. Shine (1991), On the "downward control" of extratropical diabatic circulations by eddy-induced mean zonal forces, *J. Atmos. Sci.*, *48*(4), 651–679.

Hermann, M., and A. Wiedensohler (2001), Counting efficiency of condensation particle counters at low-pressures with illustrative data from the upper troposphere, *J. Aerosol Sci.*, *32*, 975–991.

Hermann, M., F. Stratmann, M. Wilck, and A. Wiedensohler (2001), Sampling characteristics of an aircraft-borne aerosol inlet system, *J. Atmos. Oceanic Technol.*, *18*(1), 7–19.

Hintsa, E. J., et al. (1998), Troposphere-to-stratosphere transport in the lowermost stratosphere from measurements of H_2O, CO_2, N_2O and O_3, *Geophys. Res. Lett.*, *25*(14), 2655–2658.

Hipskind, R. S., G. L. Gregory, G. W. Sachse, G. F. Hill, and E. F. Danielsen (1987), Correlations between ozone and carbon monoxide in the lower stratosphere, folded tropopause, and maritime troposphere, *J. Geophys. Res.*, *92*(D2), 2121–2130.

Hoerling, M. P., T. K. Schaack, and A. J. Lenzen (1991), Global objective tropopause analysis, *Mon. Weather Rev.*, *119*(8), 1816–1831.

Hoinka, K. P., M. E. Reinhardt, and W. Metz (1993), North Atlantic air traffic within the lower stratosphere: Cruising times and corresponding emissions, *J. Geophys. Res.*, *98*(D12), 23,113–23,131.

Holton, J. R., P. H. Haynes, M. E. McIntyre, A. R. Douglass, R. B. Rood, and L. Pfister (1995), Stratosphere-troposphere exchange, *Rev. Geophys.*, *33*(4), 403–439.

Hoor, P., H. Fischer, L. Lange, J. Lelieveld, and D. Brunner (2002), Seasonal variations of mixing layer in the lowermost stratosphere as identified by the CO-O_3 correlation from in situ measurements, *J. Geophys. Res.*, *107*(D5), 4044, doi:10.1029/2000JD000289.

Hoor, P., C. Gurk, D. Brunner, M. I. Hegglin, H. Wernli, and H. Fischer (2004), Seasonality and extent of extratropical TST derived from in-situ CO measurements during SPURT, *Atmos. Chem. Phys.*, *4*, 1427–1442.

Krejci, R., J. Strom, M. de Reus, P. Hoor, J. Williams, H. Fischer, and H. C. Hansson (2003), Evolution of aerosol properties over the rain forest in Surinam, South America, observed from aircraft during the LBA-CLAIRE 98 experiment, *J. Geophys. Res.*, *108*(D18), 4561, doi:10.1029/2001JD001375.

Krol, M. C., J. Lelieveld, D. E. Oram, G. A. Sturrock, S. A. Penkett, C. A. M. Brenninkmeijer, V. Gros, J. Williams, and H. A. Scheeren (2003), Continuing emissions of methyl chloroform from Europe, *Nature*, *421*(6919), 131–135.

Lawrence, M. G., R. von Kuhlmann, M. Salzman, and P. J. Rasch (2003), The balance of effects of deep convective mixing on tropospheric ozone, *Geophys. Res. Lett.*, *30*(18), 1940, doi:10.1029/2003GL017644.

Lelieveld, J., and P. J. Crutzen (1994), Role of deep cloud convection in the ozone budget of the troposphere, *Science*, *264*(5166), 1759–1761.

Lelieveld, J., B. Bregman, F. Arnold, V. Burger, P. J. Crutzen, H. Fischer, A. Waibel, P. Siegmund, and P. F. J. van Velthoven (1997), Chemical perturbation of the lowermost stratosphere through exchange with the troposphere, *Geophys. Res. Lett.*, *24*(5), 603–606.

Liu, S. C., J. R. McAfee, and R. J. Cicerone (1984), Radon 222 and tropospheric vertical transport, *J. Geophys. Res.*, *89*(D5), 7291–7297.

Lonneman, W. A., R. L. Seila, and J. J. Bufalini (1978), Ambient air hydrocarbon concentrations in Florida, *Environ. Sci. Technol.*, *12*(4), 459–463.

McKeen, S. A., and S. C. Liu (1993), Hydrocarbon ratios and photochemical history of air masses, *Geophys. Res. Lett.*, *20*(21), 2363–2366.

McKeen, S. A., M. Trainer, E. Y. Hsie, R. K. Tallamraju, and S. C. Liu (1990), On the indirect determination of atmospheric OH radical concentrations from reactive hydrocarbon measurements, *J. Geophys. Res.*, *95*(D6), 7493–7500.

McKeen, S. A., S. C. Liu, E.-Y. Hsie, X. Lin, J. D. Bradshaw, S. Smyth, G. L. Gregory, and D. R. Blake (1996), Hydrocarbon ratios during PEM-WEST A: A model perspective, *J. Geophys. Res.*, *101*(D1), 2087–2109.

McKenna, D. S., C. J. Hord, and J. M. Kent (1995), Hydroxyl radical concentrations and Kuwait oil fire emission rates for March 1991, *J. Geophys. Res.*, *100*(D12), 26,005–26,025.

Mitchell, D. G., W. N. Mills, and J. S. Garden (1977), Multiple-curve procedure for improving precision with calibration-curve-based analyses, *Anal. Chem.*, *49*, 1655–1660.

Mühle, J., A. Zahn, C. A. M. Brenninkmeijer, V. Gros, and P. J. Crutzen (2002), Air mass classification during the INDOEX R/V *Ronald Brown* cruise using measurements of nonmethane hydrocarbons, CH_4, CO_2, CO, ^{14}CO, and $\delta^{18}O(CO)$, *J. Geophys. Res.*, *107*(D19), 8021, doi:10.1029/2001JD000730.

Mullendore, G. L., D. R. Durran, and J. R. Holton (2005), Cross-tropopause tracer transport in midlatitude convection, *J. Geophys. Res.*, *110*, D06113, doi:10.1029/2004JD005059.

Pan, L., S. Solomon, W. Randel, J. F. Lamarque, P. Hess, J. Gille, E. W. Chiou, and M. P. McCormick (1997), Hemispheric asymmetries and seasonal variations of the lowermost stratospheric water vapor and ozone derived from SAGE II data, *J. Geophys. Res.*, *102*(D23), 28,177–28,184.

Pan, L. L., W. J. Randel, B. L. Gary, M. J. Mahoney, and E. J. Hintsa (2004), Definitions and sharpness of the extratropical tropopause: A trace gas perspective, *J. Geophys. Res.*, *109*, D23103, doi:10.1029/2004JD004982.

Parrish, D. D., C. J. Hahn, E. J. Williams, R. B. Norton, F. C. Fehsenfeld, H. B. Singh, J. D. Shetter, B. W. Gandrud, and B. A. Ridley (1992), Indications of photochemical histories of Pacific air masses from measurements of atmospheric trace species at Point Arena, California, *J. Geophys. Res.*, *97*(D14), 15,883–15,901.

Poulida, O., R. R. Dickerson, and A. Heymsfield (1996), Stratosphere-troposphere exchange in a midlatitude mesoscale convective complex: 1. Observations, *J. Geophys. Res.*, *101*(D3), 6823–6836.

Prather, M. J., and D. J. Jacob (1997), A persistent imbalance in HO_x and NO_x photochemistry of the upper troposphere driven by deep tropical convection, *Geophys. Res. Lett.*, *24*(24), 3189–3192.

Ray, E. A., F. L. Moore, J. W. Elkins, G. S. Dutton, D. W. Fahey, H. Vomel, S. J. Oltmans, and K. H. Rosenlof (1999), Transport into the northern hemisphere lowermost stratosphere revealed by in situ tracer measurements, *J. Geophys. Res.*, *104*(D21), 26,565–26,580.

Ray, E. A., et al. (2004), Evidence of the effect of summertime midlatitude convection on the subtropical lower stratosphere from CRYSTAL-FACE tracer measurements, *J. Geophys. Res.*, *109*, D18304, doi:10.1029/2004JD004655.

Reed, R. J. (1955), A study of a characteristic type of upper-level frontogenesis, *J. Meteorol.*, *12*(3), 226–237.

Rhee, T. S., J. Mühle, C. A. M. Brenninkmeijer, A. Zahn, and F. Slemr (2002), Distribution of non-methane hydrocarbons in the upper troposphere and lower stratosphere in the region between central Europe and Indian Ocean during CARIBIC, paper presented at 7th Scientific Conference, Int. Global Atmos. Chem. Proj. (IGAC), Crete, Greece.

Rudolph, J., and J. J. Johnen (1990), Measurements of light atmospheric hydrocarbons over the Atlantic in regions of low biological activity, *J. Geophys. Res.*, *95*(D12), 20,583–20,591.

Scheeren, H. A., et al. (2003), Reactive organic species in the northern extratropical lowermost stratosphere: Seasonal variability and implications for OH, *J. Geophys. Res.*, *108*(D24), 4805, doi:10.1029/2003JD003650.

Spivakovsky, C. M., et al. (2000), Three-dimensional climatological distribution of tropospheric OH: Update and evaluation, *J. Geophys. Res.*, *105*(D7), 8931–8980.

Ström, J., H. Fischer, J. Lelieveld, and F. Schröder (1999), In situ measurements of microphysical properties and trace gases in two cumulonimbus anvils over western Europe, *J. Geophys. Res.*, *104*(D10), 12,221–12,226.

Talukdar, R. K., A. Mellouki, T. Gierczak, S. Barone, S. Y. Chiang, and A. R. Ravishankara (1994), Kinetics of the reactions of OH with alkanes, *Int. J. Chem. Kinet.*, *26*(10), 973–990.

Tuck, A. F., et al. (1985), 5. Strat-Tropo exchange, in *Atmospheric Ozone 1985 Assessment of Our Understanding of the Processes Controlling its Present Distribution and Change*, edited by W.G.O.R.a.M. Project, pp. 151–240, World Meteorol. Organ., Geneva, Switzerland.

Twohy, C. H., et al. (2002), Deep convection as a source of new particles in the midlatitude upper troposphere, *J. Geophys. Res.*, *107*(D21), 4560, doi:10.1029/2001JD000323.

Wang, C., and R. G. Prinn (2000), On the roles of deep convective clouds in tropospheric chemistry, *J. Geophys. Res.*, *105*(D17), 22,269–22,297.

Warneck, P. (1999), *Chemistry of the Natural Atmosphere*, 927 pp., Elsevier, New York.

Wirth, V. (2000), Thermal versus dynamical tropopause in upper-tropospheric balanced flow anomalies, *Q. J. R. Meteorol. Soc.*, *126*(562), 299–317.

Zahn, A., C. A. M. Brenninkmeijer, W. A. H. Asman, P. J. Crutzen, G. Heinrich, H. Fischer, J. W. M. Cuijpers, and P. F. J. van Velthoven (2002), Budget of O_3 and CO in the upper troposphere: CARIBIC passenger aircraft results 1997–2001, *J. Geophys. Res.*, *107*(D17), 4337, doi:10.1029/2001JD001529.

Zahn, A., C. A. M. Brenninkmeijer, and P. F. J. van Velthoven (2004), Passenger aircraft project CARIBIC 1997–2002, part I: The extratropical chemical tropopause, *Atmos. Chem. Phys. Discuss.*, *4*, 1091–1117.

C. A. M. Brenninkmeijer, H. Fischer, C. Koeppel, J. Lelieveld, T. S. Rhee, and D. H. Scharffe, Atmospheric Chemistry Division, Max Planck Institute for Chemistry, D-55020 Mainz, Germany. (rhee@mpch-mainz.mpg.de)

M. Hermann, Leibniz Institute for Tropospheric Research, D-04318 Leipzig, Germany.

J. Mühle, Scripps Institution of Oceanography, University of California, San Diego, La Jolla, CA 92093, USA.

D. E. Oram, School of Environmental Sciences, University of East Anglia, Norwich NR4 7TJ, UK.

P. F. J. van Velthoven, Royal Netherlands Meteorological Institute (KNMI), NL-3730 AE De Bilt, Netherlands.

A. Zahn, Institute of Meteorology and Climate Research, Karlsruhe University, D-76131 Karlsruhe, Germany.